

## Improvement in Prediction of the Arctic Oscillation with a Realistic Ocean Initial Condition in a CGCM

HAE-JEONG KIM

*Asia-Pacific Economic Corporation (APEC) Climate Center, Busan, South Korea*

JOONG-BAE AHN

*Division of Earth Environmental System, Pusan National University, Busan, South Korea*

(Manuscript received 30 June 2014, in final form 25 August 2015)

### ABSTRACT

This study verifies the impact of improved ocean initial conditions on the Arctic Oscillation (AO) forecast skill by assessing the one-month lead predictability of boreal winter AO using the Pusan National University (PNU) coupled general circulation model (CGCM). Hindcast experiments were performed on two versions of the model, one does not use assimilated ocean initial data (V1.0) and one does (V1.1), and the results were comparatively analyzed. The forecast skill of V1.1 was superior to that of V1.0 in terms of the correlation coefficient between the predicted and observed AO indices. In the regression analysis, V1.1 showed more realistic spatial similarities than V1.0 did in predicted sea surface temperature and atmospheric circulation fields. The authors suggest the relative importance of the contribution of the ocean initial condition to the AO forecast skill was because the ocean data assimilation increased the predictability of the AO, to some extent, through the improved interaction between tropical forcing induced by realistic sea surface temperature (SST) and atmospheric circulation. In V1.1, as in the observation, the cold equatorial Pacific SST anomalies generated the weakened tropical convection and Hadley circulation over the Pacific, resulting in a decelerated subtropical jet and accelerated polar front jet in the extratropics. The intensified polar front jet implies a stronger stratospheric polar vortex relevant to the positive AO phase; hence, surface manifestations of the reflected positive AO phase were then induced through the downward propagation of the stratospheric polar vortex. The results suggest that properly assimilated initial ocean conditions might contribute to improve the predictability of global oscillations, such as the AO, through large-scale tropical ocean–atmosphere interaction.

### 1. Introduction

The Arctic Oscillation (AO), characterized by oscillation of atmospheric pressure between the Arctic and the midlatitudes, is one of the most dominant patterns of hemispheric scale variability in the Northern Hemisphere (Thompson and Wallace 2000). Numerous studies have revealed the impacts of the AO on the boreal winter climate over the middle and high latitudes of North

America, Europe, and East Asia (e.g., Higgins et al. 2002; Kolstad et al. 2010; Park et al. 2011; Tomassini et al. 2012). The strong polar vortex confines the cold air to high latitudes closer to the Arctic and hinders the cold air from moving southward (Thompson and Wallace 2000). Thus, a mild winter across East Asia (Im and Ahn 2004; Park et al. 2011), Europe (Tomassini et al. 2012), and the eastern United States (Kolstad et al. 2010) is associated with a strong vortex and a cold winter with a weak polar vortex.

Many previous studies have insisted that the AO can be affected by external forcing, such as sea surface temperature (SST) (e.g., Hoerling et al. 2001; Kim and Ahn 2012), solar flux (e.g., Ahn and Kim 2014), snow cover (e.g., Cohen et al. 2007), sea ice (e.g., Rigor et al. 2002), and topography (e.g., Gong et al. 2004). Among these, diagnosing the impact of SST on the AO and

---

 Denotes Open Access content.

---

*Corresponding author address:* Joong-Bae Ahn, Dept. of Atmospheric Sciences, Pusan National University, 2, Busandaehak-ro 63 beon-gil, Geumjeong-gu, Busan 609-735, South Korea.  
E-mail: jbahn@pusan.ac.kr

DOI: 10.1175/JCLI-D-14-00457.1

understanding these dynamic mechanisms have been critical and long-standing issues in this regard. Hoerling et al. (2001) suggested that equatorial SST forcing is important to interannual variability and the warming trend of the AO by analyzing the data obtained from Tropical Ocean Global Atmosphere (WCRP 1985) and Global Ocean Global Atmosphere experiments. Their research showed that the changes of equatorial SSTs alter tropical rainfall and latent heating, which in turn drive changes in atmospheric circulation at higher latitudes, in particular, in the AO. According to Kryjov and Park (2007), the AO has a statistically strong connection to the ENSO throughout the whole lower stratosphere during solar minima. Li et al. (2006) explored the hemispheric pattern response induced by the SST anomaly in the tropical west and the east Pacific. They argued that the tropical western Pacific heating enhanced the annular pattern through the poleward and downstream propagation of transient eddy forcing energy; on the other hand, the eastern tropical Pacific heating produced a Pacific–North American (PNA)-like pattern with equatorward and downstream energy dissemination. To clearly differentiate the dynamics of these two warming impacts on the AO, Fletcher and Kushner (2011) investigated the atmospheric response to forced eastern tropical Pacific Ocean (TPO) and tropical Indian Ocean (TIO) warming using an atmospheric general circulation model (AGCM). They revealed that the TPO (TIO) wave response strengthened (weakened) the planetary stationary wave and thus attenuated (reinforced) the stratospheric jet, resulting in the negative (positive) AO. Lin et al. (2002) also demonstrated the response of the AO to a forcing from the tropics using a simple atmospheric model. Their study showed that eddy-mean flow interactions associated with a belt of tropical heating play an important role in the formation of the AO. They also insisted that extratropical forcing induced by tropical heating plays a substantial role in generating the AO variability. Kim and Ahn (2012) demonstrated that the third mode of the September–November mean SST over the North Pacific is a unique mode in determining the AO, and this ocean signal over the North Pacific may be a possible trigger for the AO, which, in turn, influences the local climate in the East Asia region. These investigations have emphasized the significant role of SST for the AO, although the question regarding the dynamical mechanism through which the SST induces the AO remains unclear.

Most of these studies have tried to solve these problems through AGCM experiments with various boundary conditions (e.g., Hoerling et al. 2001; Li et al. 2006; Fletcher and Kushner 2011). However, fully identifying this obscure relationship and mechanism might require

an examination using a coupled general circulation model (CGCM) (e.g., Fletcher and Kushner 2011), in which SST is evolving and interacting with atmosphere.

The forecast skill for the AO has been poor until now (Cohen et al. 2002) because the initial state of the chaotic atmosphere provides little or no information on the future state (Derome et al. 2005). The deterministic forecast of the AO is limited beyond 10 days, and many studies have tried to overcome this limitation (e.g., Kuroda 2008; Roff et al. 2011; Sun and Ahn 2014). In this respect, the AO forecast with a one-month lead time has critical importance in spite of its relatively short lead time, when considering the effect of the AO on boreal winter climate. The main interest in this study is to examine the influence of a more realistic ocean initial condition of a CGCM on the AO predictability by assessing the one-month lead predictability of a boreal winter [December–February (DJF)] AO using the Pusan National University (PNU) CGCM. The predictabilities of two versions of the PNU CGCM are compared, one does not use assimilated ocean initial data (V1.0) and one does (V1.1), and the differences between the two are discussed.

## 2. Model, data, and method

### a. Forecast system design

The atmospheric and oceanic components of the PNU CGCM, a participant model of the Asia–Pacific Economic Cooperation (APEC) Climate Center Multi-Model Ensemble Climate Prediction (<http://www.apcc21.org/eng/html/hapcc030000.html>), are the 18-vertical-layer NCAR Community Climate Model, version 3 (CCM3 at spectral T42 horizontal resolution; Hurrell et al. 1998), and the 40-vertical-layer GFDL Modular Ocean Model, version 3 (MOM3; Pacanowski and Griffies 2000), respectively. The sea ice model for the CGCM is the Elastic–Viscous–Plastic (EVP) model (Sun and Ahn 2014). The horizontal resolution of the component models is basically  $2.8125^\circ$  in latitude/longitude, but the oceanic resolution in the meridional direction is  $0.7^\circ$  at latitudes below  $30^\circ$ ;  $1.4^\circ$  at mid-latitudes between  $30^\circ$  and  $60^\circ$ ; and  $2.8^\circ$  at latitudes above  $60^\circ$  (Sun and Ahn 2014).

The two versions of the PNU CGCM, V1.0 and V1.1, are basically the same, but V1.1 includes an ocean data assimilation process when producing the initial ocean conditions for the hindcast and prediction, whereas V1.0 does not. The atmospheric initial conditions were taken from the NCEP–U.S. Department of Energy (DOE) AMIP phase 2 (AMIP-II) reanalysis (R2) (Kanamitsu et al. 2002). For generation of the initial states of the

CGCM land surface variables, first of all, an atmospheric spinup experiment was conducted by running the AGCM for 10 years starting from an arbitrary state (15 September 1978, in this study) under the given observed monthly mean climatological SST from the NOAA Optimum Interpolation Sea Surface Temperature version 2 data (Reynolds et al. 2002). The final state of the atmosphere from the spinup experiment was then taken as the initial condition of the 32-yr AMIP-type experiment running from 1978 to 2011. The land surface model output from this AMIP-type reproduction experiment was used as the initial condition of the land variables for the CGCM hindcasts.

To generate the oceanic initial conditions, the OGCM was first spun up for 100 years for the quasi-equilibrium upper ocean state by imposing monthly mean atmospheric boundary conditions taken from the R2. The restart file from the oceanic spinup experiment was used as the initial condition for the oceanic reproduction experiment from 1978 to 2011. The reproduced ocean states for the period of 1979–2010 were then used as the oceanic initial condition of PNU CGCM V1.0 hindcasts. Conversely, V1.1 utilizes the reproduced ocean states as the background field for the ocean data assimilation. Here, the variational method using a filter (VAF) (Huang 2000; Ahn et al. 2005) was applied to assimilate the Argo, XBT, TAO, and gridded NCEP Global Ocean Data Assimilation System (GODAS) temperature and salinity to the background field obtained from the reproduction simulation for generation of the initial coupled ocean conditions for V1.1. The GODAS, which already includes ocean data assimilated in 3D covering 60°S–60°N, was used in the assimilation because it is difficult to achieve dynamically and thermodynamically balanced ocean states with the sparse and irregular distribution of ocean observations (Sun and Ahn 2014). As mentioned in Sun and Ahn (2014), the purpose of these procedures in generating the initial conditions of the land surface and ocean variables is to provide sufficient memories to variables that have longer memories than atmospheric variables to minimize the shock that occurs during the initial adjustment procedure.

To compare the ocean initial condition between the two versions of the model, the mean state differences and root-mean-square error (RMSE) of SST initial conditions between the observation and two versions of the model are illustrated in Fig. 1. As shown in Fig. 1a, the SST initial condition of the V1.0 has a significant warm bias over most of the ocean areas, except over some areas in the Southern Hemisphere. However, through the ocean data assimilation, a more realistic SST initial state was produced by bias reduction (Fig. 1b). Figures 1d–f also demonstrate a marked

reduction of RMSE in the SST initial condition of V1.1 compared to V1.0. Thus, the different predictions by V1.0 and V1.1 are to be expected because of the significant differences in SST initial states.

Thereafter, two suites of seasonal prediction experiments, V1.0 and V1.1, were performed under two different oceanic initial conditions with the same atmospheric and land surface initial conditions. One-month lead hindcasts for December, January, and February initiated from November, December, and January of each year, respectively, were used to verify the one-month predictability of the AO for the 30-yr (1980–2009) boreal winter, which is recognized as the AO-active season (Thompson and Wallace 2000). Since each one-month lead hindcast initiated at each boreal winter month has its own mean model climate, the deviation from the mean of the corresponding run was defined as the anomaly.

### *b. Data and methodology*

R2 data were used as observations for comparison with model hindcasts. The monthly mean precipitation data were taken from the GPCP precipitation dataset provided by the NOAA/OAR/ESRL Physical Sciences Division (PSD) from their website (<http://www.esrl.noaa.gov/psd/>) (Adler et al. 2003). The observed SST data were obtained from the Hadley Centre Sea Ice and Sea Surface Temperature dataset (HadISST) (Rayner et al. 2003).

The AO was defined as the first mode of the combined empirical orthogonal function (CEOF) for geopotential height anomalies of each standard pressure level from the troposphere to the lower stratosphere (1000–10 hPa). The CEOF analysis is designed to empirically infer the characteristics of the space–time variations of the various field variables. This method is useful to interpret the physical meaning between multivariate data with reduced complexity in calculation (Sparnocchia et al. 2003). Prior to computing CEOF, the geopotential height field of each level was zonally averaged at every latitudinal point. The correlation coefficient between the leading principal component (PC) of CEOF and the conventional AO index with SLP was as high as the value of 0.56. Possible questions regarding the use of CEOF in defining the AO index are discussed in section 4 in detail.

## **3. Results**

This study presents the skill scores of one-month lead prediction for the AO. The monthly forecast skill of hindcasts with January initial conditions are shown as a lead time in Table 1, as an example. The contingency

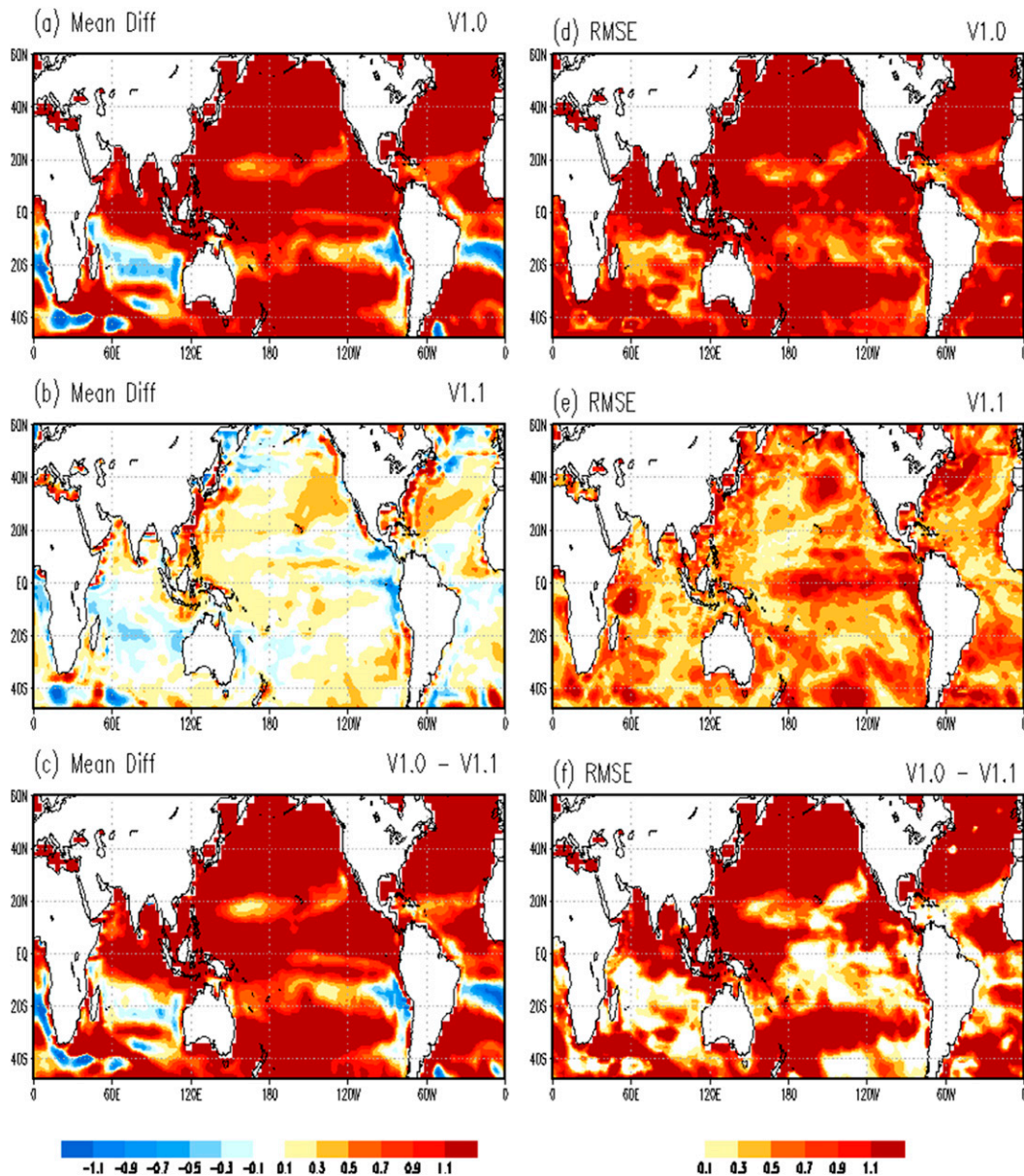


FIG. 1. (a)–(c) Mean state differences and (d)–(f) RMSE of SST initial states ( $^{\circ}\text{C}$ ) between the observation and two versions of model.

table was categorized as below normal, normal, and above normal according to a  $0.53\sigma$  threshold, and each category contained approximately 30%, 40%, and 30% of the total events, respectively. The skill shows the highest values at a one-month lead time, after which the predictabilities dropped as the lead month increased. Since one-month lead hindcasts show better AO prediction skill compared to other long-lead months, in this study, we based the following analysis on the predictability of the one-month lead hindcast. The AO for the DJF mean was analyzed by reconstructing one-

month lead data initiated from November, December, and January. The first PC of CEOF was regarded as the AO index (Fig. 2). The first mode of R2 was dominant, which accounts for 89% of the total variance for the boreal winter geopotential height. The first PC had a significant correlation coefficient of 0.56 with the conventional AO index with SLP, and both had a similar interannual variation. This relatively strong coherence between the first PC and the conventional AO index provided justification for identifying them. Therefore, the first PC could be regarded as the AO index. The AO

TABLE 1. Skill scores of the AO index for the PNU CGCM as forecast lead months (January initiated).

	Lead 1	Lead 2	Lead 3	Lead 4
Hit rate	0.47	0.37	0.40	0.40
False alarm rate	0.27	0.32	0.30	0.30
Area under curve	0.60	0.53	0.55	0.55
Heidke skill score	0.17	0.03	0.09	0.13

index used in this study can represent the variability of the whole atmosphere better since the AO is not a phenomenon confined at the surface only. The two versions of the PNU CGCM reasonably replicated the observed spatial feature of the AO characterized by a vertically meridional dipole structure with a node centered near 55°N, despite the weak strength of the dipoles (Fig. 3). Compared to V1.0, V1.1 captured the vertical location and strength of the dipole core and weak negative anomaly more realistically south of 30°N. The temporal correlation skill of the time variations for the AO between the two hindcasts and the observation were significant at the 99% level of confidence (Fig. 4). V1.1 and V1.0 had correlation coefficients of 0.69 and 0.46 with R2, respectively, which implied that V1.1 produced AO indices that were more similar with R2 than V1.0 did. The following skill score (Roff et al. 2011) was used to quantify how well V1.1 forecasted the AO index relative to V1.0:

$$\text{skill score} = \left(1 - \frac{\text{MSE}_{\text{V1.1}}}{\text{MSE}_{\text{V1.0}}}\right) \times 100, \quad (1)$$

where MSE is the mean square error for the AO index and the subscripts denote the model version.  $\text{MSE}_{\text{V1.0}}$  and  $\text{MSE}_{\text{V1.1}}$  are 1.04 and 0.59, respectively. As a result, V1.1 yielded upwards of 43% reduced forecast error in the AO index.

Since a salient difference between V1.0 and V1.1 was ocean initial state over 60°S–60°N, the questions of how much SST forecast skill was changed by improved ocean initial conditions and whether the changed SST forecast skill could contribute to the reduced forecast error in the AO index became primary interests. Figure 5 shows the spatial maps of the winter forecast skill for SST in terms of the temporal correlation coefficient between the models and the observation. The SST forecast skill consisted of significant values at the 95% confidence interval that covered most of the area for both of the models, but V1.1 was more skillful than V1.0, as shown in the figure. In addition, the prominent improvement of SST forecast skill in Fig. 5c resulting from the prescription of assimilated ocean initial conditions, statistically significant at the 95% confidence level, was found not only over the tropics but also the extratropics.

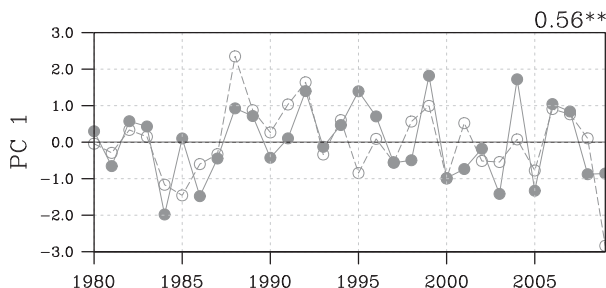


FIG. 2. The first PC time series of CEOF for geopotential anomalies from the troposphere to the lower stratosphere (closed circles) and the AO index based on the conventional EOF for SLP poleward of 20°N for wintertime (open circles).

To elucidate the possible mechanism by which reliable SST impacts more skillful AO forecast, SST and atmospheric variables, such as geopotential heights, zonal wind, SLP, 2-m temperature, and precipitation over the Northern Hemisphere were regressed onto the time variation of the AO index. Figure 6 depicts the SST patterns related to the AO for the observation and models. As shown in Fig. 6a, negative (positive) anomalies over the equator and 60°N (45°N) in the Pacific were found in R2. In the tropical Pacific, this negative anomaly has been linked to the strong the Arctic stratospheric vortex by only a few studies, although its extratropical teleconnections are less well established than those of positive SST anomalies (e.g., DeWeaver and Nigam 2002; Garfinkel et al. 2012; Zubiaurre and Calvo 2012). Also over the Atlantic in Fig. 6a, negative and positive anomalies were found over the subtropics and 45°N, respectively. In the North Atlantic, the SST regression map was dominated by a tripole pattern with negative anomalies in the subtropics and south of Greenland and a positive anomaly off the east coast of the United States (Rodwell et al. 1999) that extended to the United Kingdom. This pattern is the leading mode of SST over this region and may result in predictable oceanic influence on the North Atlantic Oscillation (NAO) (Czaja and Frankignoul 2002). Such a relation is plausible because the NAO may be a regional manifestation of the AO. As for the Indian Ocean, there was almost no distinct feature of SST connected with the AO. The only negative anomalies were found in the southern central Indian Ocean.

V1.0 showed an out-of-phase relation with the observed negative anomalies in the tropical Pacific and did not show the observed characteristics with the east–west contrast over the Indian Ocean (Fig. 6b). In the North Pacific, V1.0 showed a reasonable thermal contrast, but it was distinguished from the observation in terms of the distribution of the anomaly pair. In the North Atlantic, V1.0 simulated a tripole mode similar to the observed

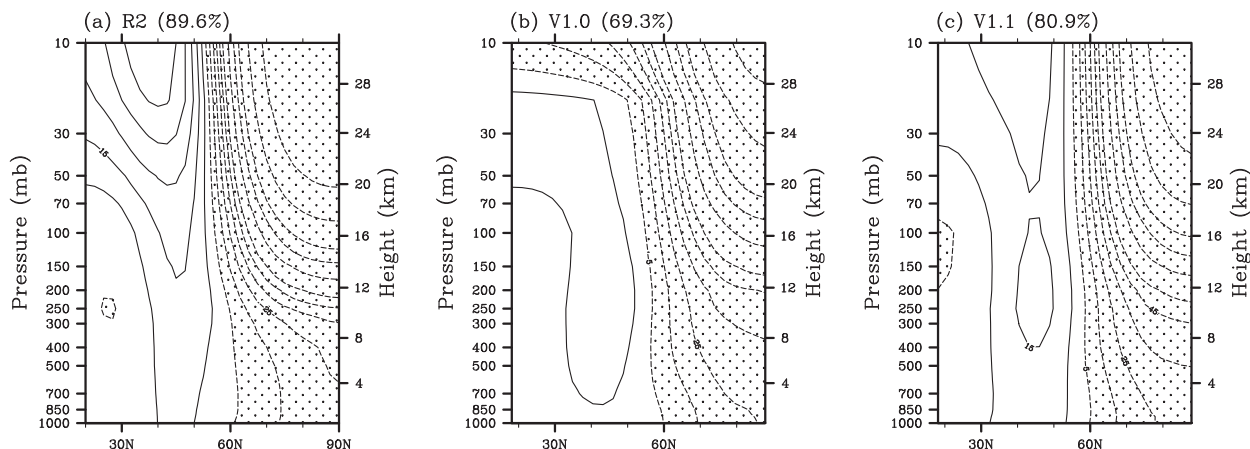


FIG. 3. Spatial structure of the first CEOF mode for geopotential height anomalies poleward of  $20^{\circ}\text{N}$  during 1980–2009, referred to here as the AO.

pattern. However, there were some deficiencies in simulating the subtropical center with the expanded positive anomaly.

In Fig. 6c, the tripole mode simulated by V1.1 resembled the observed pattern reasonably in the North Atlantic. However, the subtropical negative anomaly was slightly larger than the observation. Over the Indian Ocean, the SST signal related to the AO in V1.1 was not similar to the observation. The prediction skill of the Indian Ocean SST was rarely improved, even with V1.1, as revealed in Fig. 5. In comparison with Fig. 6b, a noticeable improvement of SST by V1.1 was found in the equatorial Pacific. The SST anomalies had an in-phase relation with the observation in this region, although the amplitude of anomalies was overestimated. As for the North Pacific, V1.1 well captured the observed feature, despite some disagreement between the observed and simulated patterns over the west coast of North America. The position of the positive core and the shape of the widthwise-stretched negative anomaly in V1.1 were more coincident with the observation than those shown in V1.0. Therefore, in this study, the AO predictability might be improved by the enhanced SST forecast skill over the Pacific.

The precipitation regressed onto the AO index revealed the diabatic heating (cooling) associated with the AO (Fig. 7). In the tropics, strongly reduced convection over the intertropical convergence zone (ITCZ) and increased precipitation over the western Pacific and the Indian Ocean, respectively, were dominant in the observed precipitation. This weakened diabatic heating over the central and eastern Pacific Ocean was caused by the cold SST anomaly in this region under the positive AO phase (see in Fig. 6). Some discrepancy between the observed data and those predicted by V1.0 was found in

not only SST but also precipitation, with the negative anomaly over  $150^{\circ}\text{E}$ – $180^{\circ}$  and the positive anomaly over  $180^{\circ}$ – $150^{\circ}\text{W}$  over the ITCZ. The deficiency was improved in V1.1 as the negative and positive anomaly enlarged and reduced, respectively. The simulated precipitation anomalies over the ITCZ were enhanced because of the impact of the ocean data assimilation, although they were underestimated in comparison with

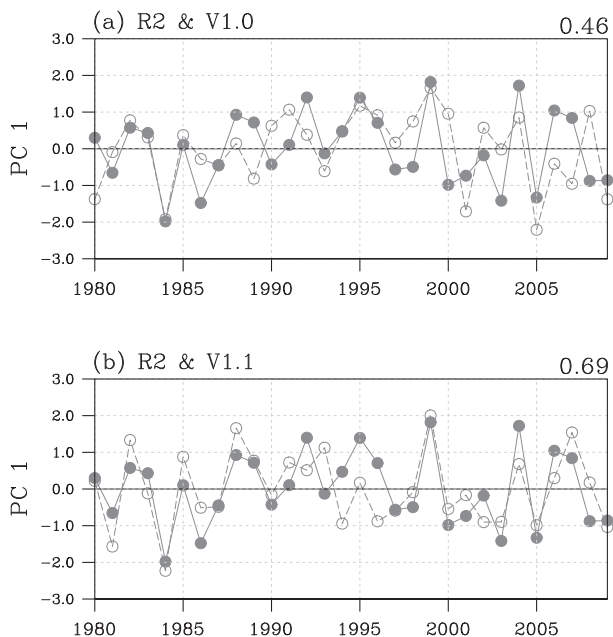


FIG. 4. Principal component time series of the first CEOF mode for geopotential height anomalies poleward of  $20^{\circ}\text{N}$  for observations (closed circles) and the two versions of the PNU CGCM (open circles) during 1980–2009. The value at the top right of each panel denotes the temporal correlation coefficient between the observation and the model.

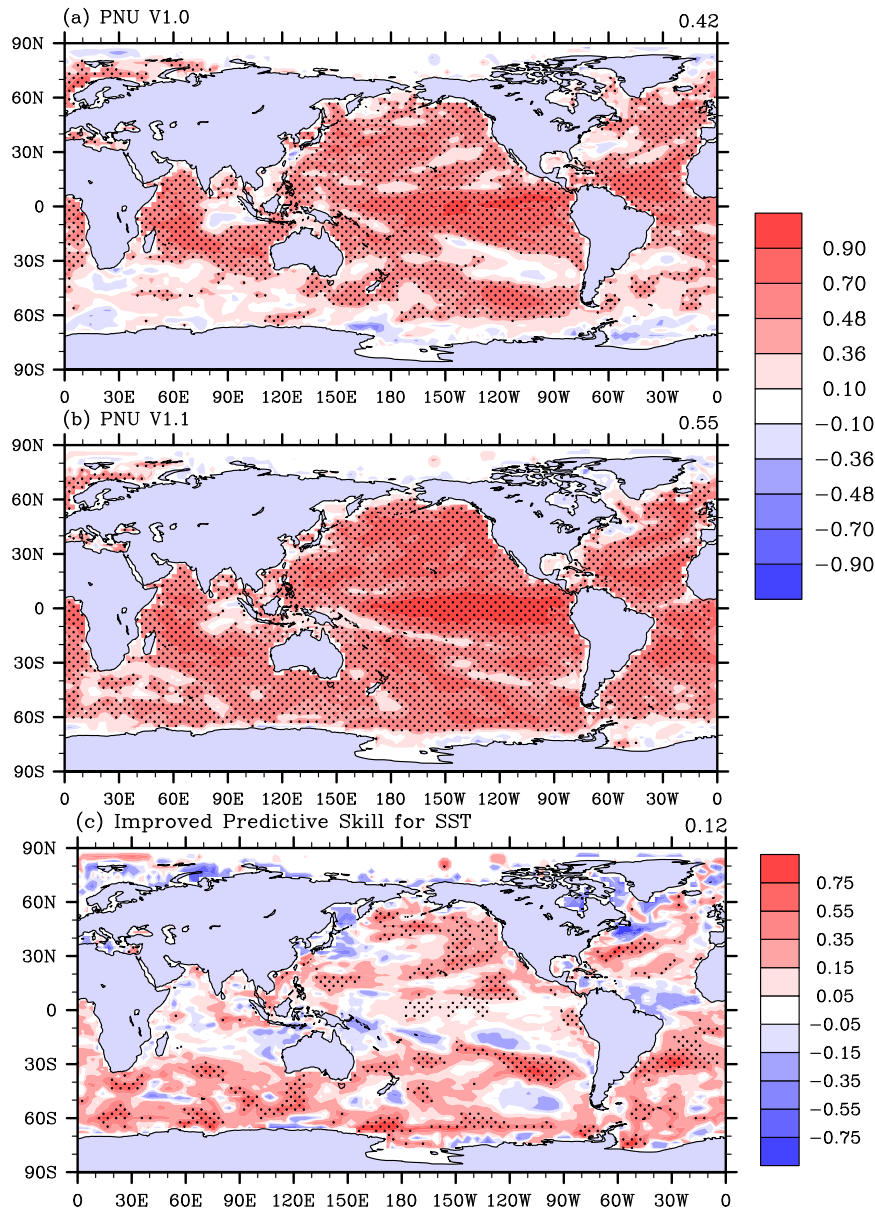


FIG. 5. Temporal correlation coefficients between (a) V1.0 and (b) V1.1 and the observations, and (c) the difference between (a) and (b) for boreal winter SST during 1980–2009. Values exceeding  $\pm 0.1$  are denoted by shading. The dotted pattern indicates the values are statistically significant over the 95% confidence level.

the observation. The reduction of precipitation over the eastern Indian Ocean in V1.0 was also improved by V1.1 with a positive sign, as in the observation. In the North Atlantic, the observed precipitation anomaly associated with the AO had a tripole-like structure (i.e., negative anomalies in the subtropical North Atlantic and positive anomalies in the high-latitude North Atlantic Ocean and the tropical western North Atlantic). This pattern was similar to the well-known precipitation response to the NAO (e.g., [Mariotti and Arkin 2007](#)), a regional

manifestation of the AO ([Thompson and Wallace 1998](#)). Both models properly simulated this tripole anomaly of the observation in the area.

The role of SST in modulating the AO is controversial ([Greatbatch 2000](#)), although many studies suggest that the role of the North Pacific in regulating extratropical climate, especially the Pacific decadal oscillation (PDO), may be related to the AO (e.g., [Sun and Wang 2006](#)). However, the relationship is dominant on the decadal time scale, since each phase of the PDO persists

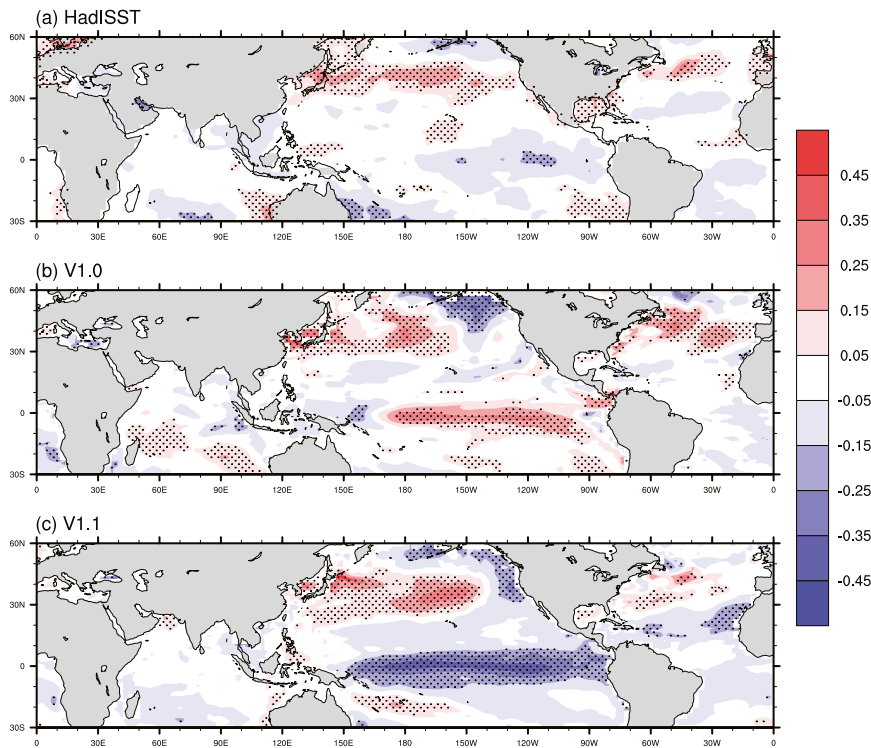


FIG. 6. SST ( $^{\circ}\text{C}$ ) regressed onto the AO index during the boreal winter for (top) observations, (middle) V1.0, and (bottom) V1.1. The dotted pattern indicates the values are statistically significant over the 95% confidence level.

for 2–3 decades. Kumar et al. (2013) demonstrated that the PDO index does not have predictive usefulness for atmospheric anomalies on seasonal prediction, because the PDO has a rather longer time scale, and other sources of variability, mainly faster-acting ones, easily overshadow the PDO's effect. Accordingly, the effects of other sources may be more noticeable than the PDO's impact because this study investigates the AO forecast and the role of the ocean at a one-month lead time. Figures 6 and 7 present evidence for the differences in AO-related SST and precipitation patterns resulting from ocean data assimilation over the tropics. In addition, it is well known that tropical SST largely determines precipitation on monthly or seasonal time scales (e.g., Krishnamurthy and Shukla 2011) and that tropical heating relative to the precipitation can drive extratropical atmospheric circulation (e.g., Greatbatch et al. 2003). The present study results therefore seem to suggest that the improvement of tropical SST accounts for the predictability source of one-month lead AO forecast.

Figure 8 shows regression maps of Hadley circulation by averaging meridional wind and vertical velocity between  $120^{\circ}\text{E}$  and  $100^{\circ}\text{W}$  over the Pacific. The Hadley circulation is known to be sensitive to meridional SST

gradients in the tropics and can act as an atmospheric “bridge” to the midlatitudes (Marshall et al. 2001). The southward retraction of the Hadley circulation with descending motion in the equatorial regions and rising motions over the subtropics in R2 was conspicuous. This weakened Hadley circulation corresponded well to the decrease of tropical convection (Fig. 7) because of the cold SST anomalies at the upward branch of the Hadley circulation (Fig. 6). It was also related with the weakened meridional temperature gradients of SST over the Pacific (as shown in Fig. 6). V1.0 did not represent this cell in terms of the upward branch near  $30^{\circ}\text{N}$  and southward flow at 300 hPa. However, the more improved SST prediction skill of V1.1 enabled it to outperform V1.0 in representing the AO-regressed Hadley circulation. The improvement was more clearly depicted in the difference of vertical and meridional circulation between V1.1 and V1.0 (Fig. 8d).

The sinking branch of the Hadley circulation interacts with the midlatitude atmospheric variability over the North Pacific (Brönnimann 2007). The jet stream, a primary interest for study of the AO in the midlatitudes, is found in the regressed 200-hPa zonal wind field on the AO index (Fig. 9). In the upper troposphere, the subtropical jet weakened over  $30^{\circ}$ – $45^{\circ}\text{N}$ , and the polar front

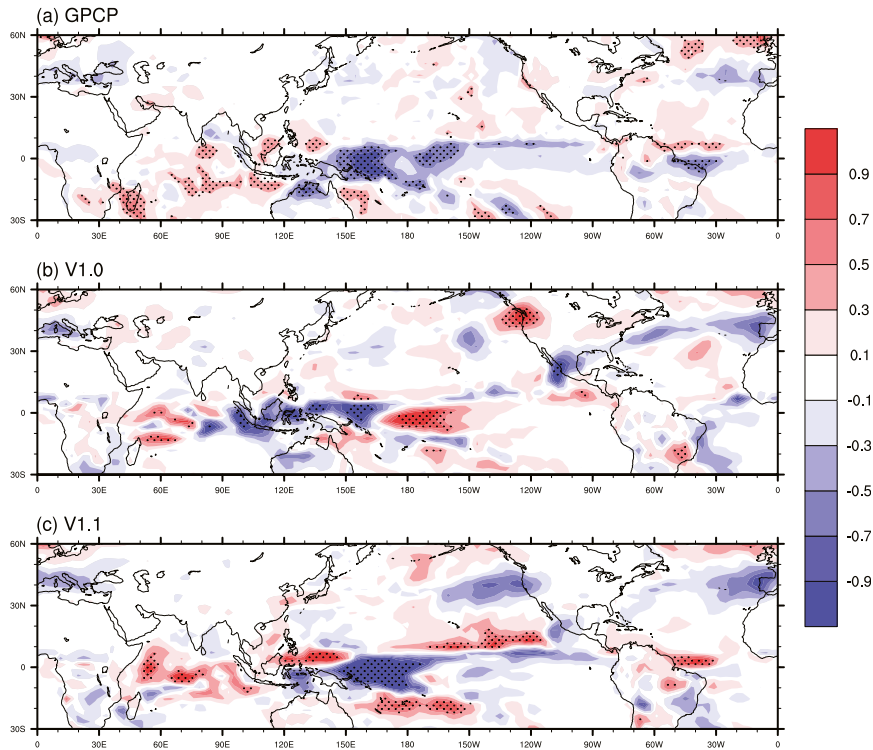


FIG. 7. As in Fig. 6, but for precipitation ( $\text{mm day}^{-1}$ ). The dotted pattern indicates the values are significant over the 95% confidence level.

jet strengthened at about  $60^\circ\text{N}$  (Fig. 9a). The subtropical jet is formed through poleward transport of angular momentum around the sinking branch of the Hadley cell (Held and Hou 1980; Lindzen and Hou 1988; Nakamura et al. 2004), partly driven by thermal convection and radiative heating in the tropics (Lee and Kim 2003). Thus, Fig. 9a suggests the weakened Hadley cell attracted the decelerated subtropical jet. The accelerated polar front jet could be explained by the fact that wave-activity dispersion with enhanced baroclinic eddy growth to the subtropical jet leads to the formation of a deep polar front jet (Nakamura et al. 2004). This is seen in more detail with Fig. 10. The overall mechanism for maintaining the subtropical and polar front jet stream is the conservation of angular momentum and eddy forcing, respectively. However, the structure of the jets also appears to be influenced by thermal contrasts. The strong vertical shear in the jets reflects a thermal wind balance consistent with the strong meridional temperature gradients, and vice versa. As shown in Fig. 6, a weakened subtropical jet and a strengthened polar front jet were also caused by the thermal wind relationship due to the meridional thermal contrasts in the North Pacific. The patterns of 200-hPa zonal wind anomalies derived by the two versions of the model were reasonably consistent with R2. However, compared with V1.0,

the zonal wind distributions simulated by V1.1 were closer to R2 with respect to the positions of the weakened subtropical jet core over the Pacific, the positive core across the Middle East, and the poleward displacement of the polar front jet boundary over western North America. The pattern correlation coefficient on the top right of the map confirms that improved SST anomalies produced more realistic subtropical and polar front jets.

The decelerated subtropical jet and the accelerated polar front jet were also supported by the regression maps of the streamfunction and baroclinicity index onto the AO reflecting the extratropical transient eddy forcing (Fig. 10). The climatological zonal wind fields from R2, V1.0, and V1.1 are also shown in Fig. 10. Following Lindzen and Farrell (1980), the baroclinicity index is defined as

$$\sigma_{\text{BI}} = \frac{f}{N} \left( \frac{du}{dz} \right) \times 0.3125, \quad (2)$$

where  $f$  and  $N$  are the Coriolis parameter and static stability, respectively, and  $du/dz$  is the change in the zonal wind velocity with height. In Fig. 10a, the negative anomalies of the baroclinicity index of R2 were apparent in the midlatitudes below  $45^\circ\text{N}$ , which delineated the

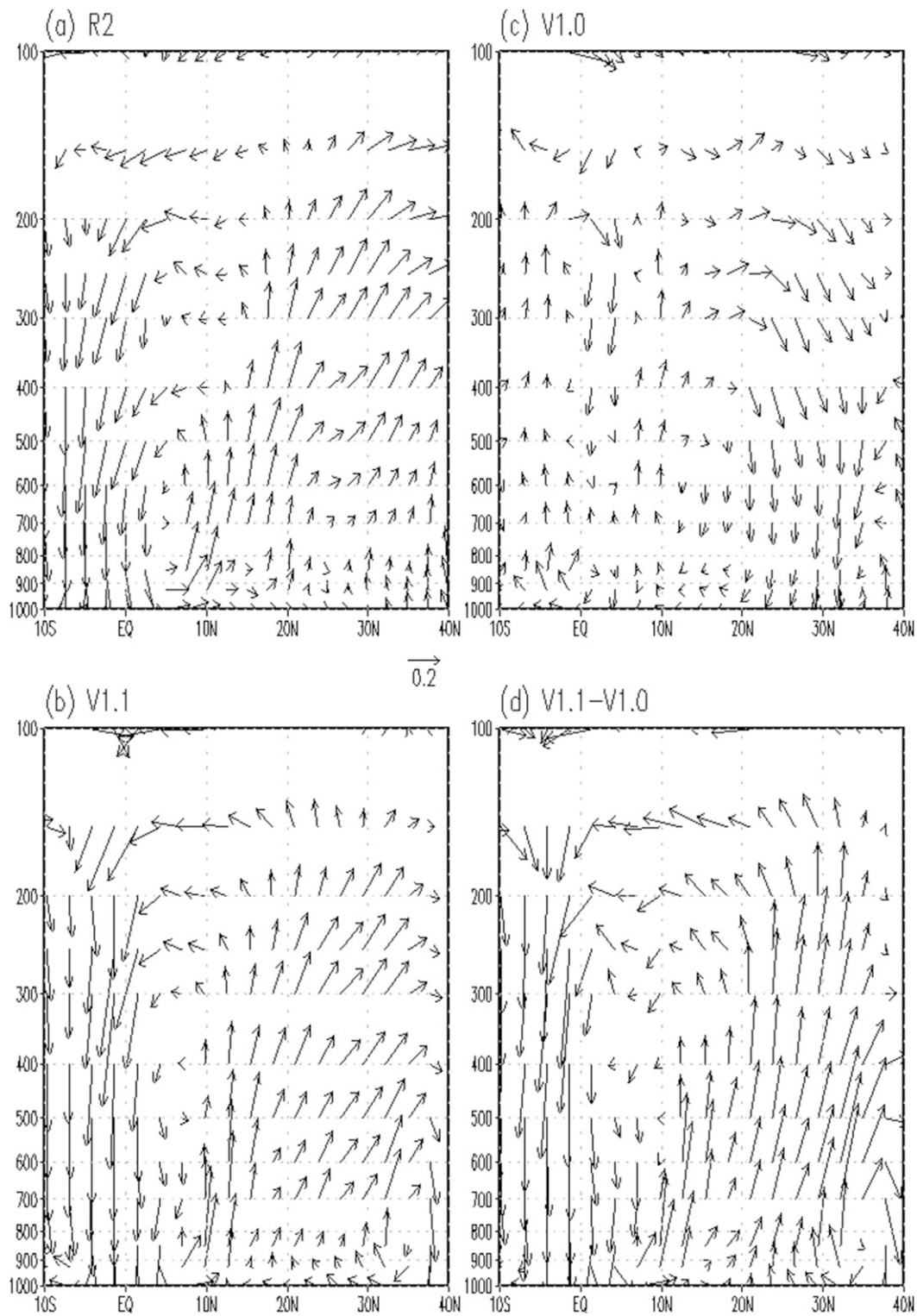


FIG. 8. Hadley circulation regressed onto the AO index during the boreal winter for (a) observations, (b) V1.1, (c) V1.0, and (d) the difference between (b) and (c). Hadley circulation is represented by averaging meridional wind and vertical velocity between 120°E and 100°W.

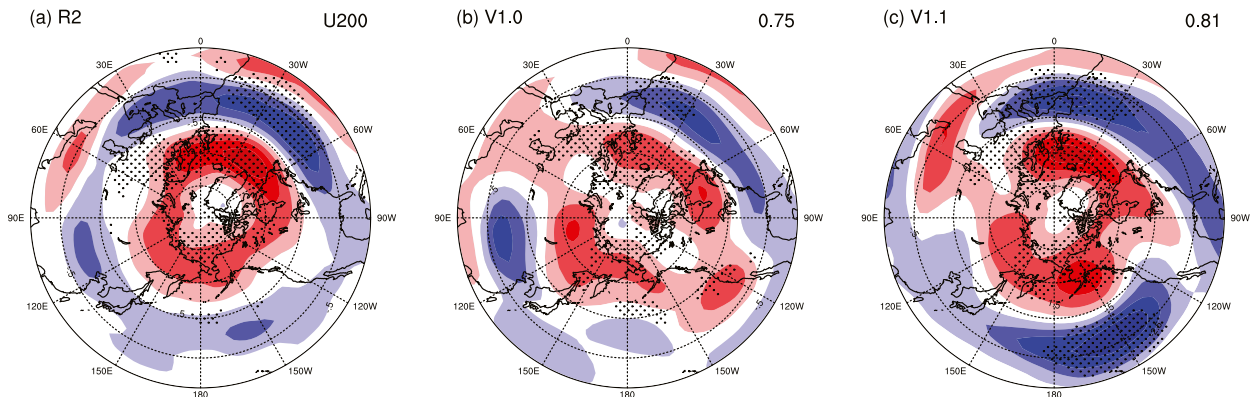


FIG. 9. Boreal winter 200-hPa zonal wind field ( $\text{m s}^{-1}$ ; shading; contour interval of  $1 \text{ m s}^{-1}$ ) regressed onto the AO index for (a) observations, (b) V1.0, and (c) V1.1. The value at the top right of (b) and (c) indicates the spatial correlation coefficient between the observation and the model. Statistically significant values at the 95% confidence level are indicated by dotted pattern.

weakened baroclinic eddies in the extratropical branch of the Hadley circulation and decelerated subtropical jet. On the other hand, the positive anomalies of the baroclinicity index were shown over about  $60^\circ\text{N}$ . These strengthened baroclinic eddies over about  $60^\circ\text{N}$  were consistent with the accelerated polar front jet, since, in the presence of a weak subtropical jet, baroclinic wave growth established the polar front jet in the midlatitudes (Lee and Kim 2003). For the streamfunction of R2 (Fig. 10b), the annular pattern with a positive signal over  $50^\circ\text{--}60^\circ\text{N}$  and a negative signal over the North Pole were remarkable. The anticyclonic streamfunction anomalies over the North Pacific were located in the vicinity of the subtropical jet. This structure hampered the maintenance of the Pacific and Atlantic jets within  $30^\circ\text{--}45^\circ\text{N}$  and strengthened the westerlies near  $50^\circ\text{N}$  by interacting with the mean flow. This indicates that the subtropical jet weakened and the polar front jet accelerated in R2 regressed onto the AO. The simulated patterns derived from V1.0 (Figs. 10c–d) and V1.1 (Figs. 10e–f) were, in general, similar to the observed features of the streamfunction, climatological zonal wind, and baroclinicity index. However, the boundary of the negative streamfunction anomalies extending northwest of the United States and the positive anomaly located in the eastern part of the North Pacific in V1.0 were northward shifted in V1.1, resulting in a more annular anomalous pattern, as in the observations. The reduced baroclinic eddy band extending zonally over the Pacific was considerably improved in V1.1.

The polar front jet is the outer edge of the polar vortex; therefore, the intensified polar jet implies a stronger polar vortex. The stratospheric polar vortex impacts the surface weather, such as 2-m temperature and SLP, anomalously during boreal winter (e.g., Thompson et al. 2002). The spatial structures of SLP and

2-m temperature associated with the AO were examined (Fig. 11). In R2, the north–south seesaw patterns of sea level pressure emerged between the midlatitude with anticyclonic anomalies and the polar region with a cyclonic anomaly. The two hindcasts and the R2 displayed a similar SLP distribution, although the models overestimated the positive center located in the Pacific region. The pattern correlation coefficient in V1.0 was just fractionally higher than that in V1.1. However, the negative anomalies extending from the Arctic to North America and the Eurasian continent were overestimated by V1.0. V1.1 reduced this bias and led to better simulation of the pattern. The surface temperature over the Northern Hemisphere can be substantially affected by the AO (e.g., Wang et al. 2005). The regression map for the 2-m temperature pattern based on the index of the AO had considerably large positive anomalies over Siberia and the United States and negative anomalies over eastern Canada and Greenland. The spatial correlation coefficient of V1.1 was considerably increased in comparison to that of V1.0. Compared to V1.0 and V1.1, this enhancement was caused by the improvement of thermal contrast between north and south Eurasia and the strong cold anomalies over the northwestern part of North America.

Stratospheric and tropospheric annular mode variations are sometimes independent of each other, but strong anomalies above the tropopause appear to favor tropospheric anomalies of the same sign since the stratospheric circulation is most variable during winter (Baldwin and Dunkerton 2001). The variation of polar vortex strength is well known as an indicator of the AO and is shown in Fig. 12. The polar vortex strength was defined as the area-averaged geopotential anomalies over the polar cap, which encompassed the area north of  $65^\circ\text{N}$ , as shown in Baldwin and Thompson (2009).

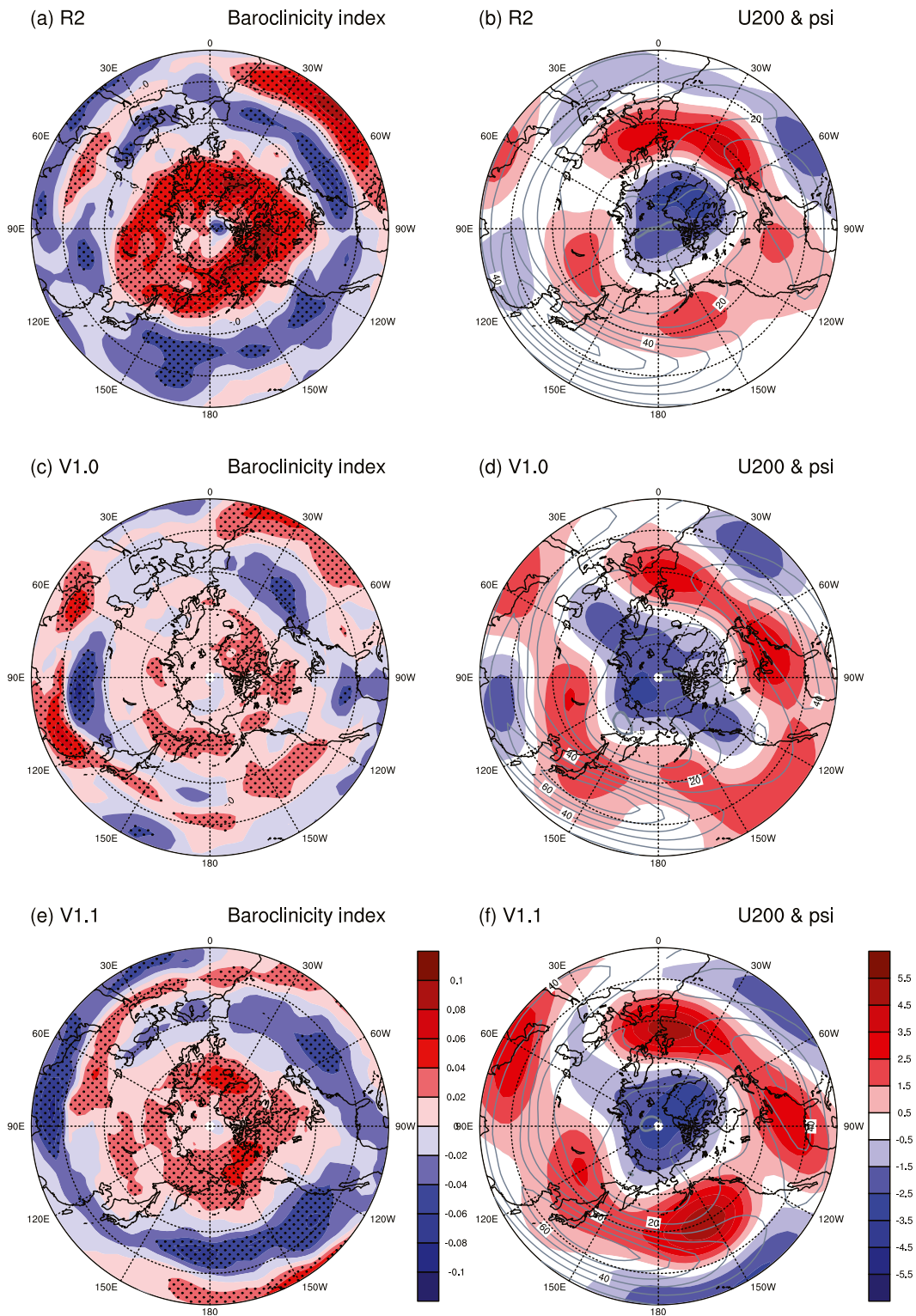


FIG. 10. (right) Climatological 200-hPa zonal wind (contour interval of  $10 \text{ m s}^{-1}$ ) and regressed streamfunction with significant values at 95% confidence level (shading;  $10^6 \text{ m}^2 \text{ s}^{-1}$ , contour interval is 1.0), and (left) regressed baroclinicity index on wintertime AO index at 200 hPa (shading; contour interval of 0.02).

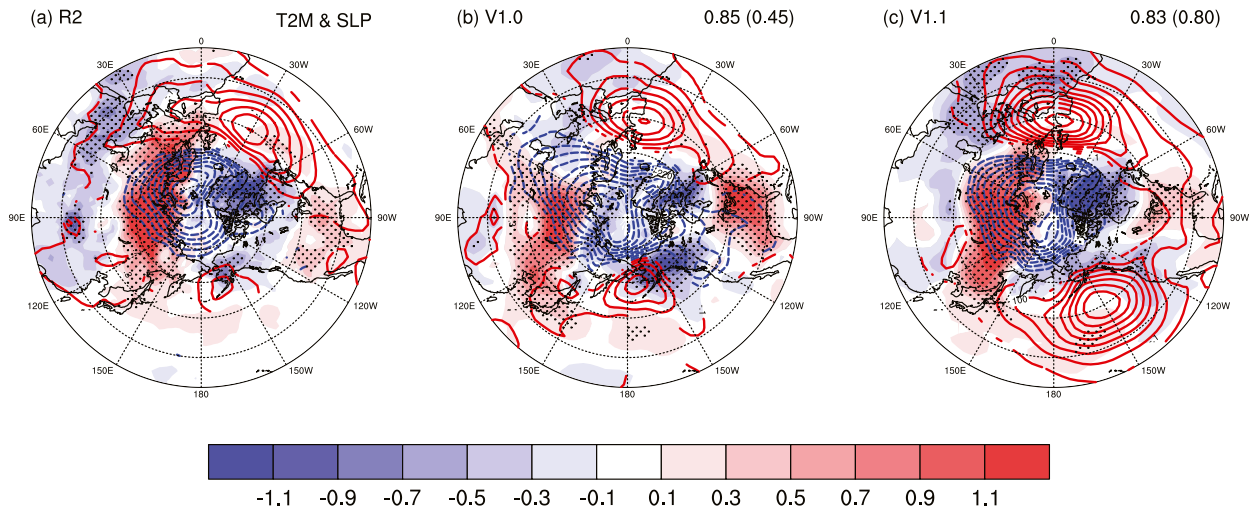


FIG. 11. As in Fig. 9, but for the SLP (contour; hPa) and 2-m temperature (shading; °C). Only statistically significant values for SLP at the 95% confidence level are drawn with thick contours, and statistically significant values for the 2-m temperature (T2M) are denoted by the dotted pattern. The value at the top right of (b) and (c) indicates the spatial correlation coefficient for the SLP between the observation and the model and the spatial correlation coefficient for 2-m temperature is given in parentheses.

Cyclostationary EOF analysis (Kim and Wu 2000) for the polar vortex strength was performed to verify the evolution of the AO. The observed pattern exhibited downward propagation of the upper-level atmosphere to the troposphere over time. The positive anomaly changed to a negative anomaly at the lower stratosphere after about 30 days. V1.1 was able to follow this migration over time and also predicted the sign change of the upper-level atmosphere. The AO signals at the low level and surface climate, shown in Fig. 12, seemed to be caused by this downward propagation of geopotential height anomalies in the NH polar vortex (Thompson et al. 2002).

Eventually, the diminution of the forecast error for the AO index, shown in the skill score, was attributed to the difference between ocean states. The improvement of the SST prediction skill resulted from more suitable ocean initial conditions, which in turn improved the predictability of the AO. That is, under the positive AO phase, the cold equatorial Pacific SST anomalies reduced the tropical convection over the Pacific, which weakened the Hadley circulation and, in turn, altered the upper-level circulation, such as the jet stream over the midlatitudes, and induced a strong stratospheric polar vortex. The surface manifestation was then reflected in the stratospheric polar vortex by propagating downward to the troposphere. This suggests that the external Rossby wave, which is weakly generated at lower latitudes arising from weakened tropical heating, tends to lead to the positive annular mode based on the argument by Lorenz and Hartmann (2003). Furthermore, our possible dynamical pathway has a similar

relationship with recent findings from Hegyi and Deng (2011) and Hegyi et al. (2014), who demonstrated that equatorial Pacific SST-driven wave anomalies associated with the eddy momentum forcing and the eddy-driven mean meridional circulation forcing result in transient responses of the stratospheric polar vortex.

#### 4. Discussion and summary

This study verified the impact of improved ocean initial conditions on one-month lead AO predictability by addressing forecast skill in terms of the basic spatial structure and temporal variation of the AO and its impact on atmospheric circulation using the PNU CGCM. To achieve this, experiments from two versions of the model, one does not use assimilated ocean initial data (V1.0) and one does (V1.1), were comparatively analyzed. The first EOF mode of geopotential height at 17 vertical levels was defined as the AO, which had a vertically meridional dipole pattern from the surface to the lower stratosphere. The temporal correlation coefficients of the AO index between the two versions of the one-month lead hindcast and observations were statistically meaningful at the 99% confidence level. As for the oceanic and atmospheric circulations relevant to the AO, the hindcast patterns exhibited good agreement with the observations in many respects. In general, the skill of the hindcast derived from V1.1 was better than that from V1.0 in terms of the circulation pattern related to the AO and the basic spatial and temporal characteristics of the AO. This may be understood in a similar context as the investigation of Barsugli and Battisti

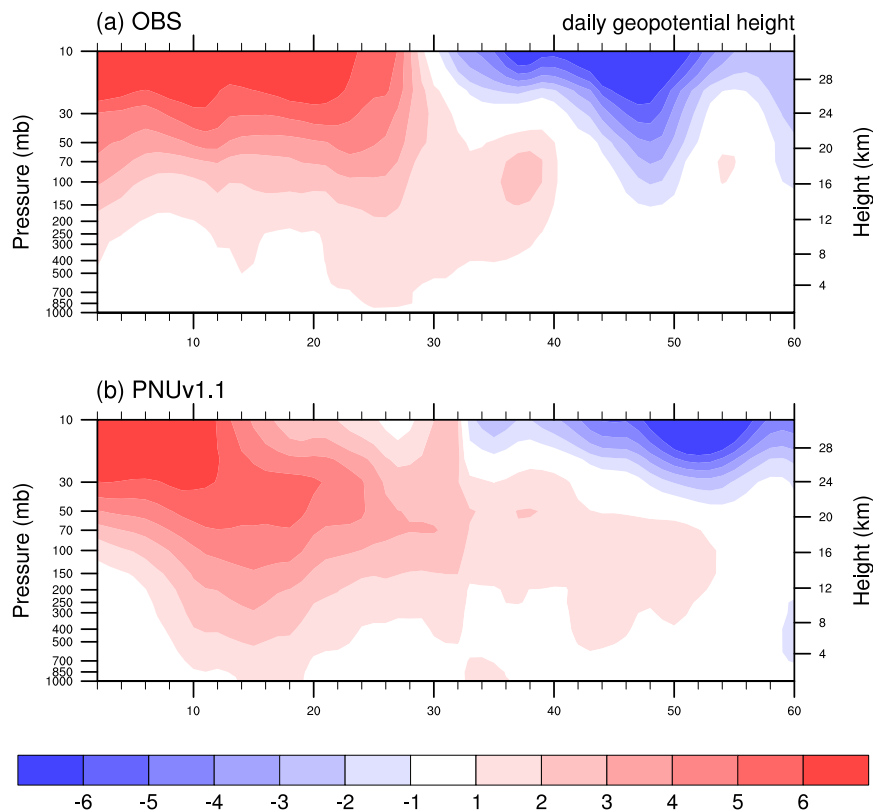


FIG. 12. Time–height development of the AO index during the 59 days from January to February. Positive values correspond to weak polar vortex and negative values to strong polar vortex.

(1998) that the improved consistency in V1.1 between the atmosphere and SST may lead to reduced thermal damping of atmospheric anomalies and thus greater persistence of the AO, which would improve skill.

This model, which uses assimilated ocean initial conditions, has a superior capability to predict global oscillations, in particular the AO with a one-month lead time. Many studies have noted that the limit of deterministic forecast for the AO is the extended-range forecast (e.g., Thompson et al. 2002; Baldwin et al. 2003; Roff et al. 2011). In this respect, this study profitably used the CGCM to fulfill the one-month forecast of the AO. Second, the improved ocean initial condition produced more realistic global SSTs and reduced forecast error in the AO index. The regression fields offered a prospect of improving the AO prediction by prescribing assimilated ocean initial conditions and supported a possible mechanism. The possible mechanism could be made more persuasive by a recent result from Hegyi et al. (2014), who introduces a first step to understand how the polar atmosphere responds to the emerging tropical SST anomalies.

Although the leading PC of CEOF used in this study had a high correlation with the conventional AO index

with SLP, its coefficient was only 0.56. Some readers may question whether using the conventional EOF based on SLP would make identification of the impact of assimilated ocean data easier. However, it is difficult to explain the long-distance mechanism from the tropical forcing to the arctic response if we confine the AO to the surface phenomenon. Therefore, we would like to capture the general features of the AO appearing at vertical levels, including the low-level stratosphere as well as that at the surface, using CEOF. Moreover, the low-level stratospheric response of the AO shown in Fig. 12 is quite possible since the equatorial Pacific SST can modulate the stratospheric polar vortex (e.g., Hegyi et al. 2014).

Our results imply that the AO variability may be governed by the Pacific SST, in conjunction with other possible mechanisms, such as the variations of solar activity (e.g., Ahn and Kim 2014), snow cover (e.g., Cohen et al. 2007), and sea ice (e.g., Rigor et al. 2002). The difference of regressed SST between V1.0, V1.1, and observations revealed a considerable difference between V1.1 and V1.0, predominantly over the tropical Pacific. This might imply that the assimilated initial ocean condition contributes to improving the

predictability of AO through tropical ocean–atmosphere interaction to some degree. However, since the winter AO and/or NAO is significantly influenced by the Arctic or North Atlantic SST and sea ice (e.g., Deser et al. 2007; Honda et al. 2009), the weak AO-related signal over the tropical Pacific observed in the present study might indicate that high-latitude oceans are still essential for the winter AO's forecast skill. Many recent studies have shown the potential interaction between tropical SST and the polar vortex (e.g., Hegyi et al. 2014; Hegyi and Deng 2011; Taguchi and Hartmann 2006). Tropical heating over the Atlantic and the Indian Ocean may also contribute to the development of the annular mode, as demonstrated in previous studies (e.g., Fletcher and Kushner 2011; Hoerling et al. 2001; Li et al. 2006; Peng et al. 2005). Nevertheless, the dynamics of this linkage in the previous studies remain under investigation. Further studies will be required to clearly elucidate the dynamical mechanism by which SST influences the AO. Moreover, since the tropical ocean–atmosphere interaction could be induced by the extratropical ocean–atmosphere interaction through the AO and PDO, the possible impact of the ocean–atmosphere interaction on the improvement of AO predictability needs to be studied further.

Only one member of the atmospheric initial condition is used in this study. The atmospheric ensemble experiments would enhance the AO response to SST forcing by eliminating the atmospheric internal variability, because the signal can be better represented by the ensemble mean as the size of the ensemble increases and the noise is averaged out. However, in order to focus on the initial ocean condition, the AO forecast skill in relation to various atmospheric ensemble members that may be associated with the internal variability is not considered in this study. Hegyi et al. (2014) also showed that the initial state and the subsequent internal variation in the extratropical atmosphere is at least as important as the type of SST forcing in determining the transient response of the stratospheric polar vortex. This means that the AO response is sensitive to the initial state; thus, the ensemble experiment may not guarantee the sole impact of ocean data assimilation on the AO forecast in this study. Nevertheless, a meaningful conclusion, whether the potential source of AO predictability comes from intrinsic atmosphere factors or SST forcing, might be reached based on the ensemble experiments.

Recently, useful levels of seasonal forecast skill of the surface North Atlantic Oscillation have been achieved by Scaife et al. (2014). They used a CGCM that has a high ocean resolution, a comprehensive representation of the stratosphere, and an interactive sea ice physics. In terms of the NAO as a regional manifestation of the

AO, their result encourages more productive challenges to forecast the AO on a seasonal time scale. It also suggests that a greatly improved prediction system could allow for plans to produce a more predictable AO forecast. Such an assessment with PNU CGCM forecasts is underway and we also expect more reliable AO prediction through future improvements in forecast techniques, such as the method for generating the initial conditions and data assimilation using PNU CGCM.

*Acknowledgments.* This work was funded by the Korea Meteorological Administration Research and Development Program under Grant KMIPA 2015-81 and Cooperative Research Program for Agriculture Science & Technology Development (Project PJ009353), Rural Development Administration, Republic of Korea. Comments from three anonymous reviewers have led to improvements in describing of the results.

#### REFERENCES

- Adler, R. F., and Coauthors, 2003: The Version-2 Global Precipitation Climatology Project (GPCP) monthly precipitation analysis (1979–present). *J. Hydrometeorol.*, **4**, 1147–1167, doi:10.1175/1525-7541(2003)004<1147:TVGPCP>2.0.CO;2.
- Ahn, J. B., and H. J. Kim, 2014: Improvement of 1-month lead predictability of the wintertime AO using a realistically varying solar constant for a CGCM. *Meteor. Appl.*, **21**, 415–418, doi:10.1002/met.1372.
- , Y. H. Yoon, E. H. Cho, and H. Oh, 2005: A study of global ocean data assimilation using VAF (in Korean). *J. Korean Soc. Oceanogr.*, **10**, 69–78.
- Baldwin, M. P., and T. J. Dunkerton, 2001: Stratospheric harbingers of anomalous weather regimes. *Science*, **294**, 581–584, doi:10.1126/science.1063315.
- , and D. W. J. Thompson, 2009: A critical comparison of stratosphere–troposphere coupling indices. *Quart. J. Roy. Meteor. Soc.*, **135**, 1661–1672, doi:10.1002/qj.479.
- , D. B. Stephenson, D. W. J. Thompson, T. J. Dunkerton, A. J. Charlton, and A. O'Neill, 2003: Stratospheric memory and extended-range weather forecasts. *Science*, **301**, 636–640, doi:10.1126/science.1087143.
- Barsugli, J. J., and D. S. Battisti, 1998: The basic effects of atmosphere–ocean thermal coupling on midlatitude variability. *J. Atmos. Sci.*, **55**, 477–493, doi:10.1175/1520-0469(1998)055<0477:TBEAO>2.0.CO;2.
- Börnimmann, S., 2007: Impact of El Niño–Southern Oscillation on European climate. *Rev. Geophys.*, **45**, RG3003, doi:10.1029/2006RG000199.
- Cohen, J., D. Salstein, and K. Saito, 2002: A dynamical framework to understand and predict the major Northern Hemisphere mode. *Geophys. Res. Lett.*, **29**, doi:10.1029/2001GL014117.
- , M. Barlow, P. J. Kushner, and K. Saito, 2007: Stratosphere–troposphere coupling and links with Eurasian land surface variability. *J. Climate*, **20**, 5335–5343, doi:10.1175/2007JCLI1725.1.
- Czaja, A., and C. Frankignoul, 2002: Observed impact of Atlantic SST anomalies on the North Atlantic Oscillation.

- J. Climate*, **15**, 606–623, doi:10.1175/1520-0442(2002)015<0606:OIOASA>2.0.CO;2.
- Derome, J., H. Lin, and G. Brunet, 2005: Seasonal forecasting with a simple general circulation model: Predictive skill in the AO and PNA. *J. Climate*, **18**, 597–609, doi:10.1175/JCLI-3289.1.
- Deser, C., R. A. Tomas, and S. Peng, 2007: The transient atmospheric circulation response to North Atlantic SST and sea ice anomalies. *J. Climate*, **20**, 4751–4767, doi:10.1175/JCLI4278.1.
- DeWeaver, E., and S. Nigam, 2002: Linearity in ENSO's atmospheric response. *J. Climate*, **15**, 2446–2461, doi:10.1175/1520-0442(2002)015<2446:LIESAR>2.0.CO;2.
- Fletcher, C. G., and P. J. Kushner, 2011: The role of linear interference in the annular mode response to tropical SST forcing. *J. Climate*, **24**, 778–794, doi:10.1175/2010JCLI3735.1.
- Garfinkel, C. I., A. H. Butler, D. W. Waugh, M. M. Hurwitz, and L. M. Polvani, 2012: Why might stratospheric sudden warmings occur with similar frequency in El Niño and La Niña winters? *J. Geophys. Res.*, **117**, D19106, doi:10.1029/2012JD017777.
- Gong, G., D. Entekhabi, and J. Cohen, 2004: Orographic constraints on a modeled Siberian snow–tropospheric–stratospheric teleconnection pathway. *J. Climate*, **17**, 1176–1189, doi:10.1175/1520-0442(2004)017<1176:OCOAMS>2.0.CO;2.
- Greatbatch, R. J., 2000: The North Atlantic Oscillation. *Stochastic Environ. Res. Risk Assess.*, **14**, 213–242, doi:10.1007/s004770000047.
- , H. Lin, J. Lu, K. A. Peterson, and J. Derome, 2003: Tropical/extratropical forcing of the AO/NAO: A corrigendum. *Geophys. Res. Lett.*, **30**, 1738, doi:10.1029/2003GL017406.
- Hegy, B. M., and Y. Deng, 2011: A dynamical fingerprint of tropical Pacific sea surface temperatures on the decadal-scale variability of cool-season Arctic precipitation. *J. Geophys. Res.*, **116**, D20121, doi:10.1029/2011JD016001.
- , —, R. X. Black, and R. Zhou, 2014: Initial transient response of the winter polar stratospheric vortex to idealized equatorial Pacific sea surface temperature anomalies in the NCAR WACCM. *J. Climate*, **27**, 2699–2713, doi:10.1175/JCLI-D-13-00289.1.
- Held, I. M., and A. Y. Hou, 1980: Nonlinear axially symmetric circulations in a nearly inviscid atmosphere. *J. Atmos. Sci.*, **37**, 515–533, doi:10.1175/1520-0469(1980)037<0515:NASCIA>2.0.CO;2.
- Higgins, R. W., A. Leetmaa, and V. E. Kousky, 2002: Relationships between climate variability and winter temperature extremes in the United States. *J. Climate*, **15**, 1555–1572, doi:10.1175/1520-0442(2002)015<1555:RBCVAW>2.0.CO;2.
- Hoerling, M. P., J. W. Hurrell, and T. Xu, 2001: Tropical origins for recent North Atlantic climate change. *Science*, **292**, 90–92, doi:10.1126/science.1058582.
- Honda, M., J. Inoue, and S. Yamane, 2009: Influence of low Arctic sea-ice minima on anomalously cold Eurasian winters. *Geophys. Res. Lett.*, **36**, L08707, doi:10.1029/2008GL037079.
- Huang, X. Y., 2000: Variational analysis using spatial filters. *Mon. Wea. Rev.*, **128**, 2588–2600, doi:10.1175/1520-0493(2000)128<2588:VAUSF>2.0.CO;2.
- Hurrell, J. W., J. J. Hack, B. A. Boville, D. L. Williamson, and J. T. Kiehl, 1998: The dynamical simulation of the NCAR Community Climate Model Version 3 (CCM3). *J. Climate*, **11**, 1207–1236, doi:10.1175/1520-0442(1998)011<1207:TDSOTN>2.0.CO;2.
- Im, E. S., and J. B. Ahn, 2004: Analysis of relationship between Korean winter temperature variability and global circulation indices (in Korean). *Asia-Pac. J. Atmos. Sci.*, **40**, 441–452.
- Kanamitsu, M., W. Ebisuzaki, J. Woollen, S. K. Yang, J. J. Hnilo, M. Fiorino, and G. L. Potter, 2002: NCEP-DEO AMIP-II Reanalysis (R-2). *Bull. Amer. Meteor. Soc.*, **83**, 1631–1643, doi:10.1175/BAMS-83-11-1631.
- Kim, H. J., and J. B. Ahn, 2012: Possible impact of the autumnal North Pacific SST and November AO on the East Asian winter temperature. *J. Geophys. Res.*, **117**, D12104, doi:10.1029/2012JD017527.
- Kim, K. Y., and Q. Wu, 2000: Optimal detection using cyclostationary EOFs. *J. Climate*, **13**, 938–950, doi:10.1175/1520-0442(2000)013<0938:ODUCE>2.0.CO;2.
- Kolstad, E. W., T. Breiteig, and A. A. Scaife, 2010: The association between stratospheric weak polar vortex events and cold air outbreaks in the Northern Hemisphere. *Quart. J. Roy. Meteor. Soc.*, **136**, 886–893, doi:10.1002/qj.620.
- Krishnamurthy, V., and J. Shukla, 2011: Predictability of the Indian monsoon in coupled general circulation models. COLA Tech. Rep. 313, 45 pp.
- Kryjov, V. N., and C. K. Park, 2007: Solar modulation of the El-Niño/Southern Oscillation impact on the Northern Hemisphere annular mode. *Geophys. Res. Lett.*, **34**, L10701, doi:10.1029/2006GL028015.
- Kumar, A., H. Wang, W. Wang, Y. Xue, and Z.-Z. Hu, 2013: Does knowing the oceanic PDO phase help predict the atmospheric anomalies in subsequent months? *J. Climate*, **26**, 1268–1285, doi:10.1175/JCLI-D-12-00057.1.
- Kuroda, Y., 2008: Role of the stratosphere on the predictability of medium-range weather forecast: A case study of winter 2003–2004. *Geophys. Res. Lett.*, **35**, L19701, doi:10.1029/2008GL034902.
- Lee, S., and H.-K. Kim, 2003: The dynamical relationship between subtropical and eddy-driven jets. *J. Atmos. Sci.*, **60**, 1490–1503, doi:10.1175/1520-0469(2003)060<1490:TDRBSA>2.0.CO;2.
- Li, S., M. Hoerling, S. Peng, and K. Weickmann, 2006: The annular response to tropical Pacific SST forcing. *J. Climate*, **19**, 1802–1819, doi:10.1175/JCLI3668.1.
- Lin, H., J. Derome, R. J. Greatbatch, K. A. Peterson, and J. Lu, 2002: Tropical links of the Arctic Oscillation. *Geophys. Res. Lett.*, **29**, doi:10.1029/2002GL015822.
- Lindzen, R. S., and B. Farrell, 1980: A simple approximate result for the maximum growth rate of baroclinic instabilities. *J. Atmos. Sci.*, **37**, 1648–1654, doi:10.1175/1520-0469(1980)037<1648:ASARFT>2.0.CO;2.
- , and A. Y. Hou, 1988: Hadley circulations for zonally averaged heating centered off the equator. *J. Atmos. Sci.*, **45**, 2416–2427, doi:10.1175/1520-0469(1988)045<2416:HCFZAH>2.0.CO;2.
- Lorenz, D. J., and D. L. Hartmann, 2003: Eddy-zonal flow feedback in the Northern Hemisphere winter. *J. Climate*, **16**, 1212–1227, doi:10.1175/1520-0442(2003)16<1212:EFFITN>2.0.CO;2.
- Mariotti, A., and P. Arkin, 2007: The North Atlantic Oscillation and oceanic precipitation variability. *Climate Dyn.*, **28**, 35–51, doi:10.1007/s00382-006-0170-4.
- Marshall, J., and Coauthors, 2001: North Atlantic climate variability: Phenomena, impacts and mechanisms. *Int. J. Climatol.*, **21**, 1863–1898, doi:10.1002/joc.693.
- Nakamura, H., T. Sampe, Y. Tanimoto, and A. Shimpo, 2004: Observed associations among storm tracks, jet streams, and midlatitude oceanic fronts. *Earth's Climate: The Ocean–Atmosphere Interaction*, C. Wang, S. P. Xie, and J. A. Carton, Eds., Amer. Geophys. Union, 329–345, doi:10.1029/147GM18.
- Pacanowski, R. C., and S. M. Griffies, 2000: MOM 3.0 Manual. NOAA/GFDL Tech. Rep., 680 pp.

- Park, T. W., C. H. Ho, and S. Yang, 2011: Relationship between Arctic Oscillation and cold surges over East Asia. *J. Climate*, **24**, 68–83, doi:10.1175/2010JCLI3529.1.
- Peng, S., W. A. Robinson, S. Li, and M. P. Hoerling, 2005: Tropical Atlantic SST forcing of coupled North Atlantic seasonal responses. *J. Climate*, **18**, 480–496, doi:10.1175/JCLI-3270.1.
- Rayner, N. A., D. E. Parker, E. B. Horton, C. K. Folland, L. V. Alexander, D. P. Rowell, E. C. Kent, and A. Kaplan, 2003: Global analyses of sea surface temperature, sea ice, and night marine air temperature since the late nineteenth century. *J. Geophys. Res.*, **108**, 4407, doi:10.1029/2002JD002670.
- Reynolds, R. W., N. A. Rayner, T. M. Smith, D. C. Stokes, and W. Wang, 2002: An improved in situ and satellite SST analysis for climate. *J. Climate*, **15**, 1609–1625, doi:10.1175/1520-0442(2002)015<1609:AIISAS>2.0.CO;2.
- Rigor, I. G., J. M. Wallace, and R. L. Colony, 2002: On the response of sea ice to the Arctic Oscillation. *J. Climate*, **15**, 2648–2663, doi:10.1175/1520-0442(2002)015<2648:ROSITT>2.0.CO;2.
- Rodwell, M. J., D. P. Rowell, and C. K. Folland, 1999: Oceanic forcing of the wintertime North Atlantic Oscillation and European climate. *Nature*, **398**, 320–323, doi:10.1038/18648.
- Roff, G., D. W. J. Thompson, and H. Hendon, 2011: Does increasing model stratospheric resolution improve extended-range forecast skill? *Geophys. Res. Lett.*, **38**, L05809, doi:10.1029/2010GL046515.
- Scaife, A. A., and Coauthors, 2014: Skillful long-range prediction of European and North American winters. *Geophys. Res. Lett.*, **41**, 2514–2519, doi:10.1002/2014GL059637.
- Sparnocchia, S., N. Pinardi, and E. Demirov, 2003: Multivariate Empirical Orthogonal Function analysis of the upper thermocline structure of the Mediterranean Sea from observations and model simulations. *Ann. Geophys.*, **21**, 167–187, doi:10.5194/angeo-21-167-2003.
- Sun, J., and H. Wang, 2006: The relationship between Arctic Oscillation and Pacific decadal oscillation on decadal timescale. *Chin. Sci. Bull.*, **51**, 75–79, doi:10.1007/s11434-004-0221-3.
- , and J. B. Ahn, 2014: Dynamical seasonal predictability of the Arctic Oscillation using a CGCM. *Int. J. Climatol.*, **35**, 1342–1353, doi:10.1002/joc.4060.
- Taguchi, M., and D. L. Hartmann, 2006: Increased occurrence of stratospheric sudden warmings during El Niño as simulated by WACCM. *J. Climate*, **19**, 324–332, doi:10.1175/JCLI3655.1.
- Thompson, D. W. J., and J. M. Wallace, 1998: The Arctic oscillation signature in the wintertime geopotential height and temperature fields. *Geophys. Res. Lett.*, **25**, 1297–1300, doi:10.1029/98GL00950.
- , and —, 2000: Annular modes in the extratropical circulation. Part I: Month-to-month variability. *J. Climate*, **13**, 1000–1016, doi:10.1175/1520-0442(2000)013<1000:AMITEC>2.0.CO;2.
- , M. P. Baldwin, and J. M. Wallace, 2002: Stratospheric connection to Northern Hemisphere wintertime weather: Implications for prediction. *J. Climate*, **15**, 1421–1428, doi:10.1175/1520-0442(2002)015<1421:SCTNHWS>2.0.CO;2.
- Tomassini, L., E. P. Gerber, M. P. Baldwin, F. Bunzel, and M. Giorgetta, 2012: The role of stratosphere–troposphere coupling in the occurrence of extreme winter cold spells over northern Europe. *J. Adv. Model. Earth. Syst.*, **4**, M00A03, doi:10.1029/2012MS000177.
- Wang, D., C. Wang, X. Yang, and J. Lu, 2005: Winter Northern Hemisphere surface air temperature variability associated with the Arctic Oscillation and North Atlantic Oscillation. *Geophys. Res. Lett.*, **32**, L16706, doi:10.1029/2005GL022952.
- WCRP 1985: Scientific plan for the Tropical Ocean and Global Atmosphere Programme. WCRP Tech. Rep. 3, 146 pp.
- Zubiaurre, I., and N. Calvo, 2012: The El Niño–Southern Oscillation (ENSO) Modoki signal in the stratosphere. *J. Geophys. Res.*, **117**, D04104, doi:10.1029/2011JD016690.